THE JOURNAL OF PHYSICAL CHEMISTRY B

pubs.acs.org/JPCB

Article

Ordering of Oblate Hard Particles between Hybrid Penetrable Walls

Candy Anquetil-Deck,* Douglas J. Cleaver,* and Paulo I. C. Teixeira*

Cite This: *J. Phys. Chem. B* 2020, 124, 7709–7716

Read Online

ACCESS | Metrics & More | Article Recommendations

ABSTRACT: We report a Monte Carlo (MC) simulation study of a model discotic liquid crystal (DLC) confined between hybrid walls with controllable penetrability. The model consists of oblate hard Gaussian overlap (HGO) particles. Particle−substrate interactions are modeled as follows: each substrate sees a particle as a disc of zero thickness and diameter D less than or equal to that of the actual particle, σ_0, embedded inside the particle and located halfway along, and perpendicular to, its minor axis. This allows us to control the anchoring properties of the substrates, from planar (edge-on) for $D \approx 0$ to homeotropic (face-on) for $D \approx \sigma_0$, which can be done independently at either substrate. Depending on the values of $D_s \equiv D/\sigma_0$ at the top (D_s^t) and bottom (D_s^b) substrates, we find domains in (D_s^b, D_s^t) space in which particle alignment is uniform planar (UP), is uniform homeotropic (UH), or varies linearly from planar at one substrate to homeotropic at the other (Lin). These domains are separated by regions of bistability (P−Lin and H−Lin), which appear to be wider than for prolate HGOs, and there may be also a small tristable (P−H−Lin) region. Results are compared with the predictions of density functional theory, implemented at the level of Onsager's second-virial approximation with Parsons-Lee rescaling. As in the case of symmetric confinement studied previously, the agreement between theory and simulation is substantially less good than for prolate HGOs: in particular, for the investigated substrate separation $L = 6\sigma_0$, the Lin configuration is never predicted. These discrepancies are likely a consequence of the fact that Onsager's theory is less accurate for discs than for rods.

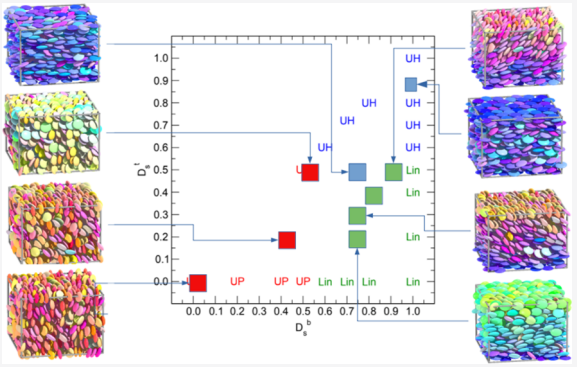

INTRODUCTION

Historically, liquid crystalline (LC) behavior was first identified in substances made up of elongated building blocks.[1] However, it has now been realized for a huge variety of molecular shapes, including plates and discs,[2] as well as at the colloidal level, e.g., in dispersions of gibbsite[3] or clay[4] particles. Such discotic liquid crystals (DLCs) may exhibit semiconducting properties, with promising applications in the photovoltaic industry.[5] They are also effective as lubricants, outperforming hydrocarbons in some conditions.[6] In all these practical settings, an understanding of LCs at surfaces and interfaces is paramount, which combined with sheer curiosity, has spawned a number of theoretical, computational, and experimental studies.

On the theory side, only hard-body models have been used. Harnau and Dietrich extended Onsager's second-virial theory to treat infinitely thin hard discs with continuous orientations[7] and binary mixtures of hard platelets with restricted orientations[8] at a hard wall. More recently, Kapanowski and Abram[9] found, also on the basis of Onsager's second-virial theory, that hard platelets will order biaxially at a hard wall only if the bulk phase itself is biaxial. A more sophisticated, fundamental-measure (FM) density functional theory (DFT) of infinitely thin hard platelets, both pure and mixed, was developed by Schmidt and co-workers.[10] This was applied to the isotropic−nematic (I−N) interface of suspensions of colloidal platelets[11,12] and to the capillary nematization of thin hard discs between parallel hard walls,[13] with results generally superior to those of Onsager's second-virial theory.

On the side of computer simulations, Piñeiro *et al.*[14] carried out a *NPT* and Gibbs ensemble Monte Carlo (MC) investigation of hard cut spheres of aspect ratio $L/D = 0.1$ in a slab geometry between either hard walls that exclude the particles completely or "adsorbent" walls that exclude only the particles' centers of mass. Avendaño *et al.*[15] simulated soft-repulsive rings between parallel, soft-repulsive walls, with results that are in stark contrast to the behavior of convex DLCs. Finally, other numerical studies of confined DLCs have employed the popular Gay−Berne (GB) model and more complex wall−particle interactions.[16−20] In all of the above, only symmetric confinement has been assumed, i.e., where both substrates induce the same anchoring.

Received: June 3, 2020
Revised: July 30, 2020
Published: July 31, 2020

https://dx.doi.org/10.1021/acs.jpcb.0c05027
J. Phys. Chem. B 2020, 124, 7709–7716

In a recent paper,[21] we started a research program aimed at establishing the design principles for DLCs in confined environments. We chose a simple (for ease of use and generality) hard-body model that allows one to switch between different types of anchoring in either symmetric or hybrid systems by tuning a physically transparent parameter. Our model consists of oblate hard Gaussian overlap (HGO) particles sandwiched between parallel planar substrates: each substrate sees a particle as a disc of zero thickness and diameter D less than or equal to that of the actual particle, σ_0, embedded inside the particle and located halfway along, and perpendicular to, its minor axis; the anchoring induced by a given substrate is planar (edge-on) for $D \approx 0$ and homeotropic (face-on) for $D \approx \sigma_0$. In the present paper, we consider hybrid confinement in the simplest case in which either substrate of a slit-like pore may induce a different anchoring. These are the boundary conditions relevant to important LC applications such as twisted-nematic[22] or hybrid-aligned[23] displays and are also realized, e.g., in nanometrically thin 5CB films spun-cast onto silicon wafers.[24]

This paper is organized as follows: first, we describe our model. Then, details of the computer simulations are given, followed by a section where results are presented and compared with the predictions of the previously published theory.[21] Finally, we give some conclusions.

MODEL

As in previous works,[21,25−27] we consider a purely steric microscopic model of uniaxial particles represented by the hard Gaussian overlap (HGO) potential:[28]

$$U^{\mathrm{HGO}} = \begin{cases} 0 \text{ if } r_{ij} \geq \sigma(\hat{\mathbf{r}}_{ij}, \hat{\mathbf{u}}_i, \hat{\mathbf{u}}_j) \\ \infty \text{ if } r_{ij} < \sigma(\hat{\mathbf{r}}_{ij}, \hat{\mathbf{u}}_i, \hat{\mathbf{u}}_j) \end{cases}$$

where $\hat{\mathbf{u}}_i$ and $\hat{\mathbf{u}}_j$ are the orientations of particles i and j, $\hat{\mathbf{r}}_{ij}$ is the interparticle unit vector, and $\sigma(\hat{\mathbf{r}}_{ij}, \hat{\mathbf{u}}_i, \hat{\mathbf{u}}_j)$ is the contact distance, given by

$$\sigma(\hat{\mathbf{r}}_{ij}, \hat{\mathbf{u}}_i, \hat{\mathbf{u}}_j) = \sigma_0 \left[1 - \frac{\chi}{2} \left[\frac{(\hat{\mathbf{r}}_{ij}\cdot\hat{\mathbf{u}}_i + \hat{\mathbf{r}}_{ij}\cdot\hat{\mathbf{u}}_j)^2}{1 + \chi(\hat{\mathbf{u}}_i\cdot\hat{\mathbf{u}}_j)} + \frac{(\hat{\mathbf{r}}_{ij}\cdot\hat{\mathbf{u}}_i - \hat{\mathbf{r}}_{ij}\cdot\hat{\mathbf{u}}_j)^2}{1 - \chi(\hat{\mathbf{u}}_i\cdot\hat{\mathbf{u}}_j)} \right] \right]^{-1/2} \quad (1)$$

The parameter χ is set by the particle length-to-breadth ratio $\kappa = \sigma_L/\sigma_0$ via

$$\chi = \frac{\kappa^2 - 1}{\kappa^2 + 1} \quad (2)$$

In this study, we consider disc-shaped, i.e., $\kappa < 1$, particles. For moderate κ, the HGO model is a good approximation to hard ellipsoids (HEs);[29−31] furthermore, their virial coefficients (and thus their equations of state, at least at low to moderate densities) are very similar.[32,33]

From a computational point of view, HGOs have the considerable advantage over HEs that the distance of closest approach between two particles is given in closed form.[34] Particle−substrate interactions are now modeled, as in ref 13, by a hard disc−wall (HDW) potential (see Figure 1)

$$\beta V^{\mathrm{HDW}}(z, \theta) = \begin{cases} 0 & \text{if } |z - z_0^{\alpha}| \geq \frac{1}{2} D \sin\theta \\ \infty & \text{if } |z - z_0^{\alpha}| < \frac{1}{2} D \sin\theta \end{cases} \quad (3)$$

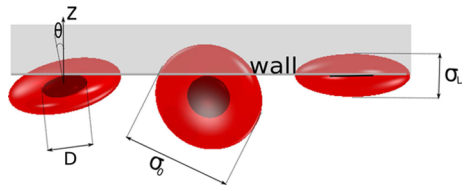

Figure 1. HDW potential: The wall sees a particle as a hard disc of diameter D, which need not equal σ_0. Varying D between 0 and σ_0 is equivalent to changing the degree of side-group penetrability into the confining substrates and hence the substrate's anchoring properties.

where $\beta = 1/k_B T$, θ is the polar angle of the HGO orientation vector, and the z-axis has been chosen to be perpendicular to the substrates, located at $z = z_0^{\alpha}$ (α = 1,2). According to eq 3, particles see each other as HGOs, but the substrates see a particle as an infinitely thin disc of diameter D (which need not be the same at both substrates or in different regions of each substrate). This is the oblate-particle version of the hard needle-wall potential of our earlier works:[25−27,35] physically, $0 < D < \sigma_0$ means that the particles are able to embed their side and end groups, but not the whole width of their cores, into the bounding walls. In an experimental situation, this might be achieved by manipulating the density, orientation, or chemical affinity of an adsorbed surface layer. In what follows, the substrate is characterized using the dimensionless parameter $D_s = D/\sigma_0$; as shown in ref 21, this allows us to set the anchoring at either wall as either homeotropic (face-on) for $D_s \lesssim 1$ or planar degenerate (edge-on) for $D_s \ll 1$, although anchoring strengths cannot be finely controlled in this way (more on this later).

The theory in refs 21 and[25−27] describes the orientational structure of an LC film in terms of the following orientational order parameters, calculated in the laboratory-fixed frame[36]

$$\eta(z) = \langle P_2(\cos\theta) \rangle = Q_{zz} \quad (4)$$

$$\varepsilon(z) = \langle \sin 2\theta \sin\phi \rangle = \frac{4}{3} Q_{yz} \quad (5)$$

$$\nu(z) = \langle \sin 2\theta \cos\phi \rangle = \frac{4}{3} Q_{xz} \quad (6)$$

$$\varsigma(z) = \langle \sin^2\theta \cos 2\phi \rangle = \frac{2}{3}(Q_{xx} - Q_{yy}) \quad (7)$$

$$\tau(z) = \langle \sin^2\theta \sin 2\phi \rangle = \frac{4}{3} Q_{xy} \quad (8)$$

where $\langle A(z) \rangle = \int A(z, \omega) \hat{f}(z, \omega)\, d\omega$, with $\hat{f}(z, \omega)$ being the orientational distribution function. Here, $\omega_i = (\theta, \phi)$ denote the polar and azimuthal angles describing the orientation of the short axis of a particle. These equations allow us to write down the five independent components of the nematic order parameter tensor, $Q_{\alpha\beta} = \left\langle \frac{1}{2}(3\hat{\omega}_\alpha \hat{\omega}_\beta - \delta_{\alpha\beta}) \right\rangle$, in terms of the order parameters in the laboratory-fixed frame

$$Q_{xx} = -\frac{1}{2}\eta + \frac{3}{4}\varsigma \quad (9)$$

https://dx.doi.org/10.1021/acs.jpcb.0c05027
J. Phys. Chem. B 2020, 124, 7709−7716

$$Q_{yy} = -\frac{1}{2}\eta - \frac{3}{4}\varsigma \tag{10}$$

$$Q_{zz} = \eta \tag{11}$$

$$Q_{xy} = \frac{3}{4}\tau \tag{12}$$

$$Q_{yz} = \frac{3}{4}\varepsilon \tag{13}$$

$$Q_{xz} = \frac{3}{4}\nu \tag{14}$$

$Q_{\alpha\beta}$ give the fraction of molecules oriented along the z-axis (Q_{zz}), along the bisectors of the yz-, xz-, and xy-quadrants (Q_{yz}, Q_{xz}, and Q_{xy}, respectively), and the difference between the fractions of molecules oriented along the x- and y-axes ($Q_{xx} - Q_{yy}$).

In an earlier paper,[27] we characterized the overall nematic order (both uniaxial and biaxial) and the biaxial order of the film using the two scalar order parameters q and β^2 originally proposed by Hess *et al.*[37]

$$q(z) = \left[\frac{2}{3}\mathrm{Tr}\mathbf{Q}^2(z)\right]^{1/2} \tag{15}$$

$$\beta^2(z) = 1 - 6\frac{[\mathrm{Tr}\mathbf{Q}(z)^3]^2}{[\mathrm{Tr}\mathbf{Q}(z)^2]^3} \tag{16}$$

(where Tr denotes the trace of a tensor), as well as some of the individual components of $Q_{\alpha\beta}$. In a more recent work,[21] we found that β^2 is very noisy when $\mathrm{Tr}\mathbf{Q} \approx 0$, i.e., in weakly ordered regions, which may obscure any truly biaxial behavior. As we shall see in Results, the $\mathbf{Q}$ tensor we obtain, be it from theory or from simulation, is almost always approximately diagonal; hence, it is appropriate to characterize biaxiality using $Q_{xx} - Q_{yy}$ instead. On the other hand, q turns out to be a convenient measure of the degree of order with respect to a spatially varying preferential direction of alignment, as is the case in our hybrid films. Q_{zz}, as usual, tells us whether alignment is homeotropic ($Q_{zz} > 0$) or planar ($Q_{zz} < 0$).

SIMULATIONS

The effect of confinement was studied by performing *NVT* MC simulations of $N = 864$ HGO particles of length-to-breadth ratio $\kappa = 0.345$, sandwiched between two hybrid substrates a distance $L_z = 6\sigma_0$ apart. Periodic boundary conditions were imposed in the x and y directions. In simulation as well as in theory, the reduced bulk density $\rho^* = \rho\sigma_0^3$ (which we shall often refer to as "bulk density" or simply "density") is defined as just the number of particles divided by the volume of the simulation box: it is not the density of the bulk fluid coexisting with the confined fluid. Each system was initialized at a low density ($\rho^* = 1.5$) and gently compressed by decreasing the box dimensions L_x and L_y while keeping the substrate separation L_z fixed. At each density, run lengths of 1 million MC sweeps (where one sweep represents one attempted move per particle) were performed, with averages and profiles being accumulated for the final 500,000 sweeps. It is difficult to say how long a run needs to be to guarantee equilibration, but blocks of 500−1000 time steps or MC cycles are typical (for an N-atom system, one MC cycle is N attempted moves).[38] For our system, 500,000 attempted moves per particle were performed during equilibration, which is in line with the above: a system composed of 864 HGO particles is estimated to need between 432,000 and 864,000 attempted moves per particles to reach equilibration. Analysis has been performed by dividing the stored system configurations into 100 equidistant constant-z slices and computing averages of relevant observables in each slice. This yields profiles of quantities such as the number density $\rho^*(z)$, from which structural changes can be assessed. Orientational order parameter profiles have also been calculated, particularly

$$\langle Q_{zz}(z)\rangle = \frac{1}{N(z)}\sum_{i=1}^{N(z)}\left(\frac{3}{2}u_{i,z}^2 - \frac{1}{2}\right) \tag{17}$$

which measures the variation across the confined films of orientational order measured with respect to the substrate normal. Here, $N(z)$ is the instantaneous occupancy of the relevant slice and θ_i is the angle between the substrate normal (i.e., the z-axis) and the particle orientation $\mathbf{u}_i$.

RESULTS

All results presented are for $\kappa = 0.345$ and substrate separation $L_z = 6\sigma_0$. In what follows, D_s^b and D_s^t denote, respectively, the dimensionless thin disc diameter at the bottom (left in figures) and top (right in figures) substrates. Theoretical calculations have been performed as described in ref 21.

Figure 2 plots $\langle q(z)\rangle$, the spatial average of $q(z)$ across the films, as a function of the reduced bulk density $\rho^* = \rho\sigma_0^3$ for the

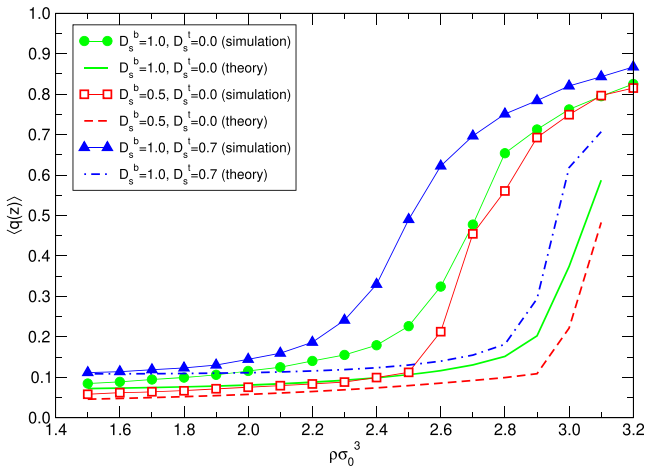

Figure 2. Total nematic order parameter $q(z)$ averaged over the whole film vs bulk density for all (D_s^b, D_s^t) studied. Lines are from theory, and symbols are from simulation (the thin lines connecting the symbols are just to guide the eye). The variation appears to be always continuous.

films discussed below. As in ref 27, $\langle q(z)\rangle$ is a continuous, increasing function of $\rho\sigma_0^3$. It does not vanish even at the lowest densities investigated because the substrates always induce some orientational order. In our earlier paper,[21] we estimated the bulk I−N transition for HGOs of elongation $\kappa = 0.345$ to occur at $\rho^* \approx 2.5$ (from simulation) or $\rho^* \approx 2.9$ (from theory).

It is interesting to note that $\langle q(z)\rangle$ begins to rise at a slightly lower density of $\rho^* \approx 2.4$ (from simulation) or $\rho^* \approx 2.8$ (from theory) if the film is uniform homeotropic ($D_s^b = 1.0$, $D_s^t = 0.7$). On the other hand, this rise is postponed to higher densities if the film is uniform planar ($D_s^b = 0.5$, $D_s^t = 0.0$). These shifts in the apparent I−N transition density are well captured by theory.

$\langle Q_{xx}(z) - Q_{yy}(z)\rangle$, the spatial average of the biaxial order parameter $\langle Q_{xx}(z) - Q_{yy}(z)(z)\rangle$ across the same films, is

https://dx.doi.org/10.1021/acs.jpcb.0c05027
J. Phys. Chem. B 2020, 124, 7709−7716

likewise plotted vs ρ^* in Figure 3. As expected, there is no biaxiality if the film is uniform homeotropic ($D_s^b = 1.0$, $D_s^t = 0.7$).

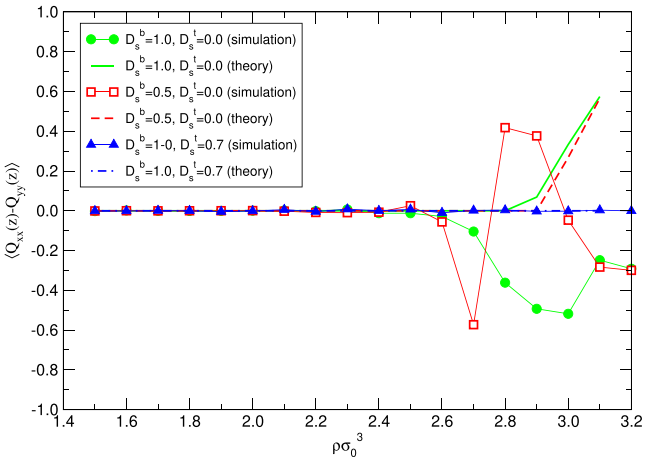

Figure 3. Biaxial nematic order parameter $Q_{xx}(z) - Q_{yy}(z)$ averaged over the whole film vs bulk density for all (D_s^b, D_s^t) studied. Lines are from theory, and symbols are from simulation (the thin lines connecting the symbols are just to guide the eye). The biaxiality is very small when ($D_s^b = 1.0$ and $D_s^t \geq 0.6$), for which the alignment is face-on throughout the whole film.

In contrast, for uniform planar alignment ($D_s^b = 0.5$, $D_s^t = 0.0$), there is a clear biaxial signature but it fluctuates a lot. This suggests that, as was the case with some symmetric-aligned films,[21] although the minor axes of particles are instantaneously aligned along some direction in the xy-plane, that direction itself changes on the scale of a few MC steps. Finally, a film whose alignment changes continuously from homeotropic at one substrate to planar at the other ($D_s^b = 1.0$, $D_s^t = 0.0$) exhibits a more regular biaxial signal.

Figure 4 shows the reduced density $\rho^*(z)$ and Figure 5 shows the total nematic order parameter $q(z)$, with respect to the substrate normal $Q_{zz}(z)$ and biaxiality order parameter $Q_{xx}(z) - Q_{yy}(z)$, for the most extreme asymmetric confinement, corresponding to $D_s^b = 1.0$ and $D_s^t = 0.0$. At low bulk densities $\rho^*(z)$ has a single peak at $z \approx D_s^b/2$ near the bottom substrate, a much higher peak right at the top substrate, $z \approx L_z$, and a dip at about $z \approx L_z - \sigma_0/2$. Both peaks are associated with freely rotating HGOs that either do not penetrate or fully penetrate the left (bottom) or right (top) substrates, respectively. The dip appears as the gap between a first layer of particles sliding edge-on into the right (top) substrate and the bulk of the film.

As ρ^* is increased, two new density peaks appear, one at a distance $\sim 0.05\sigma_0$ from the left substrate and the other at a distance $0.9\sigma_0$ from the right substrate; the former eventually grows higher than the peak at $z \approx D_s^b/2$.

Agreement between theory and simulation is fair for bulk densities $\rho^* = 1.6$ and $\rho^* = 2.5$ but deteriorates dramatically for $\rho^* = 3.1$, for which theory predicts very strong layering with periodicity $\sim\sigma_0$ emanating from the right (recall this is the planar-anchoring) substrate, which is not borne out by simulation.

Predictions for the order parameters are even less accurate: already for $\rho^* = 2.5$, theory underestimates the extent of order in the film. Then, for $\rho^* = 3.1$, theory predicts that about three quarters of the film starting from the planar-anchoring (right) substrate are edge-on, and the remainder are face-on, with a "wall defect" of reduced $q(z)$ of thickness $\sim\sigma_0$ in between.

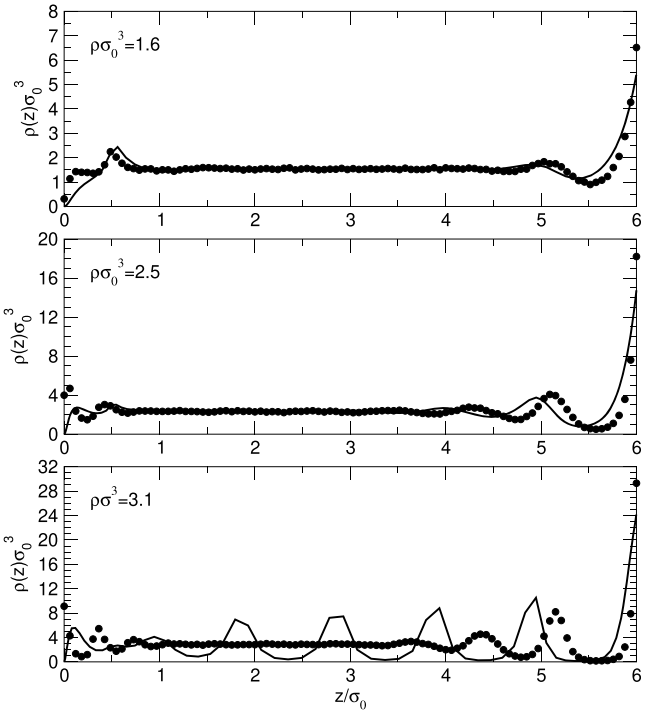

Figure 4. Reduced density profile $\rho^*(z)$ from theory (lines) and simulation (symbols) of the maximally hybrid film corresponding to $D_s^b = 1.0$ (left, or bottom, substrate) and $D_s^t = 0.0$ (right, or top, substrate) for reduced bulk densities $\rho^* = 1.6$ (top), 2.5 (center), and 3.1 (bottom). The lowest density lies in the I phase, the intermediate density in the I–N transition region, and the highest density in the N phase.

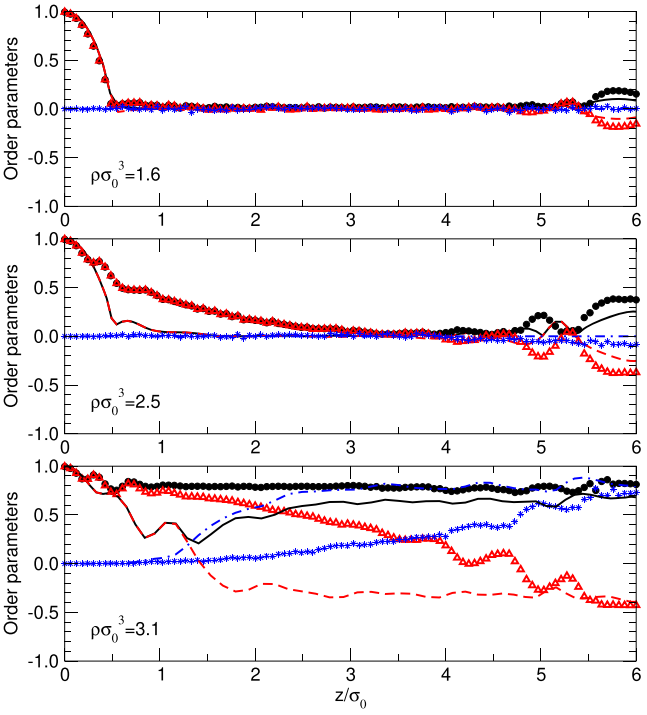

Figure 5. Order parameters $q(z)$ black solid lines and black filled circles), $Q_{zz}(z)$ (red dashed lines and red open triangles), and $Q_{xx} - Q_{yy}$ (blue dot-dashed lines and blue stars) for the system in Figure 4. Lines are from theory, and symbols are from simulation.

https://dx.doi.org/10.1021/acs.jpcb.0c05027
J. Phys. Chem. B 2020, 124, 7709–7716

In contrast, simulation sees a linear variation of $Q_{zz}(z)$ across the film, which, combined with a nearly-uniform $q(z)$, instead implies a gradual rotation of the direction of preferential alignment. This effect is similar to what we observed for thin films of rod-like HGOs also in maximally hybrid confinement,[26] on the basis of which we expect the agreement between theory and simulation to improve for larger substrate separations L.

The above configuration, which we call Lin, is adopted if D_s^b and D_s^t are sufficiently different (this statement will be quantified below). Otherwise, the film will be uniform homeotropic (UH, Figures 6 and 7) if D_s^b and D_s^t are both greater than about 0.5 or

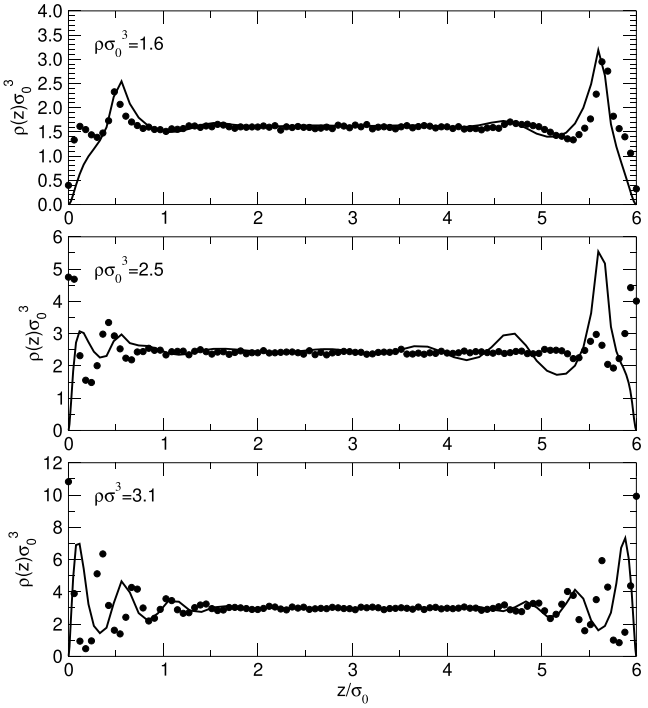

Figure 6. Reduced density profile $\rho^*(z)$ from theory (lines) and simulation (symbols) of the hybrid film corresponding to $D_s^b = 1.0$ (left, or bottom, substrate) and $D_s^t = 0.7$ (right, or top, substrate) for reduced bulk densities $\rho^* = 1.6$ (top), 2.5 (center), and 3.1 (bottom). The lowest density lies in the I phase, the intermediate density in the I−N transition region, and the highest density in the N phase.

uniform planar (UP, Figures 8 and 9) if D_s^b and D_s^t are both less than about 0.5. In these cases, the agreement between theory and simulation is comparable to that seen for symmetric films.[21]

Specifically in the UP case, for which there is more pronounced layering, theory overestimates the density peak spacing as well as their height. For the substrate separation $L_z = 6\sigma_0$ considered here, theory is never able to reproduce the Lin configuration.

Figure 10 shows snapshots of the simulated systems in Figures 4−9.

Figure 11 summarizes our simulation findings in (D_s^b, D_s^t) space. It is seen that UP (edge-on) alignment dominates when D_s^b and D_s^t are both substantially smaller than 1, whereas UH (face-on) alignment is obtained for D_s^b and D_s^t both close to 1. When $D_s^b \gg D_s^t$ ($D_s^b \ll D_s^t$), there is homeotropic (planar) alignment at the bottom (top) substrate, and the direction of preferential alignment rotates linearly from one substrate to the next (Lin).

The UP, UH, and Lin domains are separated by what appear to be regions of bistability, i.e., where one can observe more than

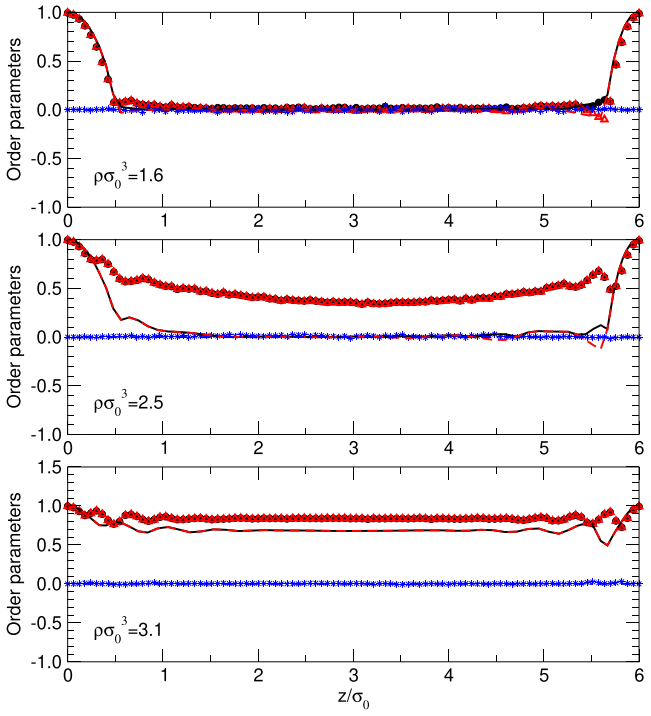

Figure 7. Order parameters $q(z)$ (black solid lines and black filled circles), $Q_{zz}(z)$ (red dashed lines and red open triangles), and $Q_{xx} - Q_{yy}$ (blue dot-dashed lines and blue stars) for the system in Figure 6. Lines are from theory, and symbols are from simulation.

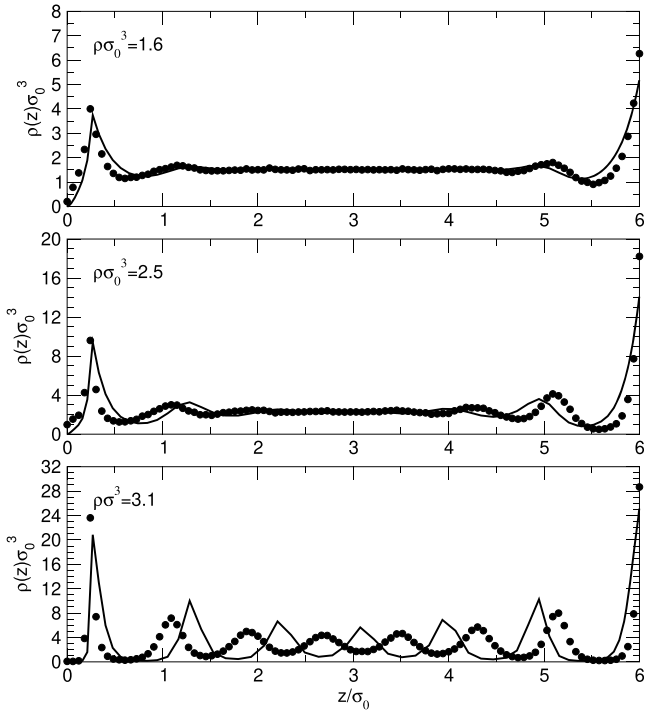

Figure 8. Reduced density profile $\rho^*(z)$ from theory (lines) and simulation (symbols) of the hybrid film corresponding to $D_s^b = 0.5$ (left, or bottom, substrate) and $D_s^t = 0.0$ (right, or top, substrate) for reduced bulk densities $\rho^* = 1.6$ (top), 2.5 (center), and 3.1 (bottom). The lowest density lies in the I phase, the intermediate density in the I−N transition region, and the highest density in the N phase.

one behavior, depending on the history and/or initial conditions. Moreover, the Lin domain cannot reach the main

https://dx.doi.org/10.1021/acs.jpcb.0c05027
J. Phys. Chem. B 2020, 124, 7709−7716

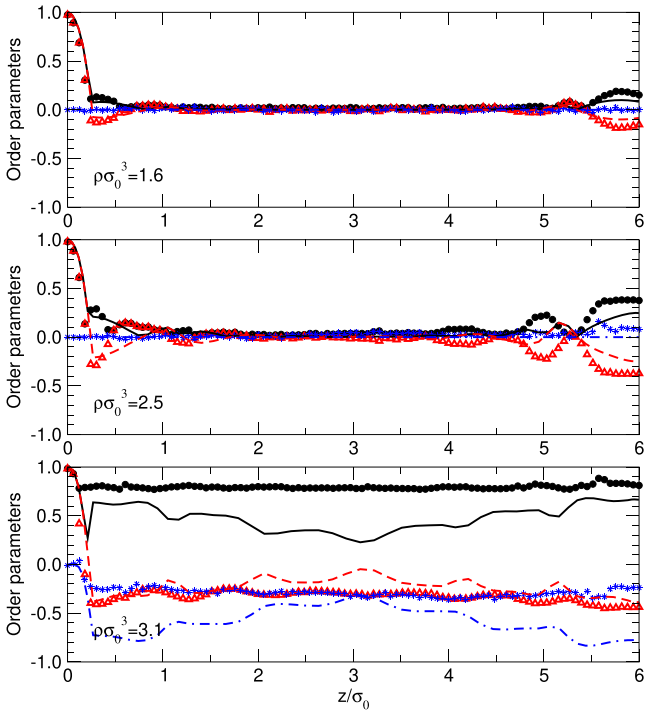

Figure 9. Order parameters $q(z)$ (black solid lines and black filled circles), $Q_{zz}(z)$ (red dashed lines and red open triangles), and $Q_{xx} - Q_{yy}$ (blue dot-dashed lines and blue stars) for the system in Figure 8. Lines are from theory, and symbols are from simulation.

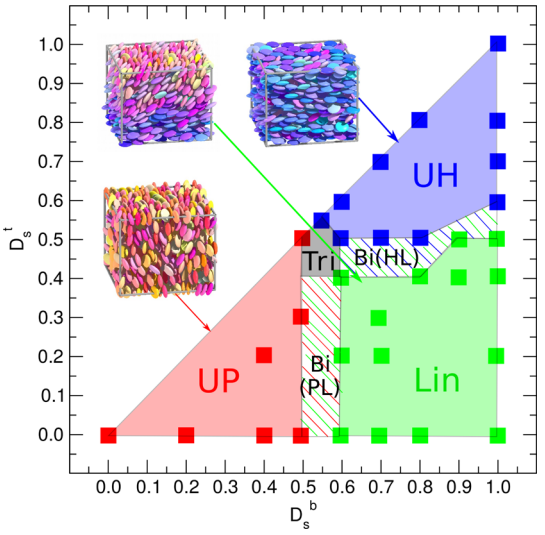

Figure 11. Regime diagram for a hybrid-confined HGO film of thickness $L_z = 6\sigma_0$. UH: uniform homeotropic (face-on); UP: uniform planar (edge-on); Lin: linear rotation from homeotropic to planar; Bi: bistable (conjectured); Tri: tristable (conjectured). The upper half of the diagram can be obtained by exchanging D_s^b and D_s^t in the lower half and is therefore not shown.

diagonal as equal substrate treatments only yield uniform alignment states. It does, however, get very close, and there may be a (presumably small) tristability domain on the main diagonal. We are currently running further simulations and theoretical calculations to verify this hypothetical scenario.

The regime diagram in Figure 11 is asymmetric. In particular, the UP domain is larger than the UH domain, which suggests that planar anchoring is stronger than homeotropic anchoring. The HDW potential used here does not allow very precise control of the anchoring strengths, so we can only speculate why this is so. For hard rods, Schmidt *et al.*[39] argued that the planar wall should have a stronger aligning effect as it will align even an individual rod: the only way a rod can be close to an impenetrable wall is by being parallel to it. This should be manifested in a higher value of the nematic order parameter close to such a wall at low densities, when most of the film is still

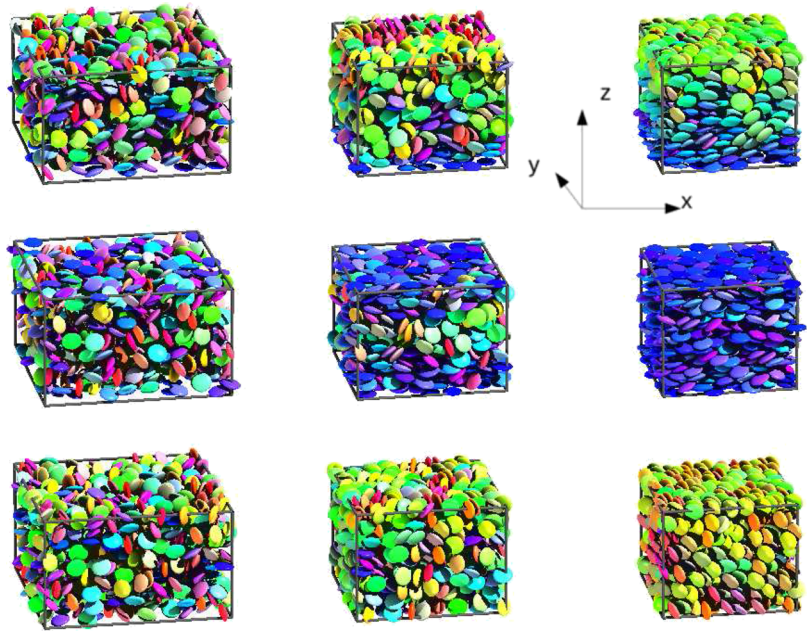

Figure 10. Configuration snapshots of hybrid-confined oblate HGO films. First row: $D_s^b = 1.0$ and $D_s^t = 0.0$; second row: $D_s^b = 1.0$ and $D_s^t = 0.7$; third row: $D_s^b = 0.5$ and $D_s^t = 0.0$. Left column: $\rho^* = 1.6$ (I); middle column; $\rho^* = 2.5$ (I + N); right column: $\rho^* = 3.1$ (N). The substrates (not shown) are at the top and bottom box faces. Colors give the orientation of a particle's short axis: along x (red), along y (green), or along z (blue).

https://dx.doi.org/10.1021/acs.jpcb.0c05027
J. Phys. Chem. B 2020, 124, 7709−7716

isotropic, which indeed we found for prolate HGOs.[27] Now for oblate HGOs, the nematic order parameter is always larger at the homeotropic wall for exactly the same reason: the only way a disc can be close to a wall is by lying flat on it. But a face-on layer of oblate HGOs has a very low density, much lower than that of an edge-on layer, because each HGO takes up a lot of wall area. This is in contrast with prolate HGOs, which each takes up very little wall area, and thus can pack more densely, when perpendicular to the wall. So, for oblate HGOs, we have a very high degree of alignment of very few face-on particles at the homeotropic wall and a somewhat lower degree of alignment of many more edge-on particles at the planar wall. Contrast this with the prolate HGOs, for which we have a higher density at the homeotropic wall than at the planar wall, coupled with degrees of alignment that are not very different at either wall.[26,27] We conjecture that it is the ability to pack more densely that makes the edge-on anchoring of oblate HGOs stronger than their face-on anchoring. However, this dominance of one wall over the other appears to be rather marginal; recall that, in the case of prolate HGOs, no firm conclusions could be drawn in this respect.[27]

CONCLUSIONS

In this paper, we have presented a combined MC simulation and DFT treatment of an oblate HGO particle fluid in hybrid confinement between parallel substrates. The anchoring can be tuned at either substrate by varying the extent to which a particle is allowed to penetrate it. If the anchorings at the two substrates are not too different, then a state of uniform alignment, either planar (UP) or homeotropic (UH), is realized. Otherwise, there is a linear variation from planar alignment at one substrate to homeotropic alignment at the other. These states correspond to domains in the space of anchoring parameters (D_s^b, D_s^t). In between these domains, there may be regions of bistability, or even of tristability, where the configuration that is actually realized may depend on system history and/or initial conditions. Such bi- or tristable regions appear to be larger than for prolate HGOs and are currently under investigation.

The Onsager approximation, combined with a simple Parsons-Lee density rescaling, previously applied to confined prolate HGO particle fluids, can yield semiquantitative predictions for the density and orientational distribution in the UP and UH states, for the relatively large elongation $\kappa = 0.345$. However, at higher densities, and especially close to substrates that induce planar (edge-on) alignment, the theory substantially overestimates the extent of layering as it also does in the case of symmetric confinement.[21] It is also not able to reproduce the Lin state for a substrate separation $L_z = 6\sigma_0$. On the basis of a similar result for prolate HGOs of elongation $\kappa = 3$,[26] we expect the theory to become more accurate for larger substrate separations. It might therefore still be a useful tool to model technological applications, in which typical film thicknesses are much greater than just a few particle diameters. We are currently working on implementing Schmidt's FM-DFT[10] for our particular choice of substrates.

AUTHOR INFORMATION

Corresponding Authors

Candy Anquetil-Deck − *Department of Chemical Engineering, Norwegian University of Sciene and Technology, NO-7491 Trondheim, Norway*; Email: candy.deck@ntnu.no

Douglas J. Cleaver − *Materials and Engineering Researh Institute, Sheffield Hallam University Pond Street, Sheffield S1 1WB, United Kingdom*; orcid.org/0000-0002-4278-0098; Email: D.J.Cleaver@shu.a.uk

Paulo I. C. Teixeira − *ISEL−Instituto Superior de Engenharia de Lisboa, Instituto Politécnico de Lisboa, 1959-007 Lisboa, Portugal; Centro de Física Teórica e Computacional, Faculdade de Ciências, Universidade de Lisboa, 1749-016 Lisboa, Portugal*; orcid.org/0000-0003-2315-2261; Phone: +44 114 2253055; Email: piteixeira@fc.ul.pt

Complete contact information is available at: https://pubs.acs.org/10.1021/acs.jpcb.0c05027

Notes

The authors declare no competing financial interest.

ACKNOWLEDGMENTS

We acknowledge financial support from the Portuguese Foundation for Science and Technology (FCT) under contracts nos. UIDB/00618/2020 and UIDP/00618/2020 and from Instituto Politécnico de Lisboa under project IPL/2019/DISCONEDGE_ISEL.

REFERENCES

(1) Collings, P. J. *Liquid Crystals: Nature's Delicate Phase of Matter*; 2nd edition. Princeton University Press: Princeton (NJ), 2001.

(2) Tschierske, C. Micro-Segregation, Molecular Shape and Molecular Topology - Partners for the Design of Liquid Crystalline Materials with Complex Mesophase Morphologies. *J. Mater. Chem.* **2001**, *11*, 2647−2671.

(3) van der Kooij, F. M.; Lekkerkerker, H. N. W. Formation of Nematic Liquid Crystals in Suspensions of Hard Colloidal Platelets. *J. Phys. Chem. B.* **1998**, *102*, 7829−7832.

(4) Pizzey, C.; van Duijneveldt, J.; Klein, S. Liquid Crystal Clay Composites. *Mol. Cryst. Liq. Cryst.* **2010**, *409*, 51−57.

(5) Zou, C.; Wang, J.; Wang, M.; Wu, Y.; Gu, K.; Shen, Z.; Xiong, G.; Yang, H.; Jiang, L.; Ikeda, T. Patterning of Discotic Liquid Crystals with Tunable Molecular Orientation for Electronic Applications. *Small* **2018**, *14*, 1800557.

(6) Bushby, R. J.; Kawata, K. Liquid Crystals that Affected the World: Discotic Liquid Crystals. *Liq. Cryst.* **2011**, *38*, 1415−1426.

(7) Harnau, L.; Dietrich, S. Fluids of Platelike Particles near a Hard Wall. *Phys. Rev. E* **2002**, *65*, No. 021505.

(8) Harnau, L.; Dietrich, S. Wetting and Capillary Nematization of Binary Hard-Platelet and Hard-Rod Fluids. *Phys. Rev. E* **2002**, *66*, No. 051702.

(9) Kapanowski, A.; Abram, M. Model of Hard Spheroplatelets near a Hard Wall. *Phys. Rev. E* **2014**, *89*, No. 062503.

(10) Esztermann, A.; Reich, H.; Schmidt, M. Density Functional Theory for Colloidal Mixtures of Hard Platelets, Rods, and Spheres. *Phys. Rev. E* **2006**, *73*, No. 011409.

(11) van der Beek, D.; Reich, H.; van der Schoot, P.; Dijkstra, M.; Schilling, T.; Vink, R.; Schmidt, M.; van Roij, R.; Lekkerkerker, H. Isotropic-Nematic Interface and Wetting in Suspensions of Colloidal Platelets. *Phys. Rev. Lett.* **2006**, *97*, No. 087801.

(12) Reich, H.; Dijkstra, M.; van Roij, R.; Schmidt, M. Entropic Wetting and the Free Isotropic-Nematic Interface of Hard Colloidal Platelets. *J. Phys. Chem. B* **2007**, *111*, 7825−7835.

(13) Reich, H.; Schmidt, M. Capillary Nematization of Hard Colloidal Platelets Confined Between two Parallel Hard Walls. *J. Phys.: Condens. Matter* **2007**, *19*, 326103.

(14) Piñeiro, M. M.; Galindo, A.; Parry, A. O. Surface Ordering and Capillary Phenomena of Confined Hard Cut-Sphere Particles. *Soft Matter* **2007**, *3*, 768−778.

(15) Avendaño, C.; Jackson, G.; Wensink, H. H. Nanorings in Planar Confinement: the Role of Repulsive Surfaces on the Formation of Lacuna Smectics. *Mol. Phys.* **2018**, *116*, 2901−2910.

(16) Bellier-Castella, L.; Caprion, D.; Ryckaert, J.-P. Surface Ordering of Diskotic Liquid Crystals. *J. Chem. Phys.* **2004**, *121*, 4874−4883.
(17) Caprion, D. Discotic Molecules in Cylindrical Nanopores: A Monte Carlo Study. *Eur. Phys. J. E: Soft Matter Biol. Phys.* **2009**, *28*, 305−313.
(18) Busselez, R.; Cerclier, C. V.; Ndao, M.; Ghou, A.; Lefort, R.; Morineau, D. Discotic Columnar Liquid Crystal Studied in the Bulk and Nanoconfined States by Molecular Dynamics Simulation. *J. Chem. Phys.* **2014**, *141*, 134902.
(19) Salgado-Blanco, D.; Mendoza, C. I.; Chávez-Rojo, M. A.; Moreno-Razo, J. A.; Díaz-Herrera, E. Influence of Anchoring in the Phase Behaviour of Discotic Liquid Crystals. *Soft Matter* **2018**, *14*, 2846−2859.
(20) Salgado-Blanco, D.; Díaz-Herrera, E.; Mendoza, C. I. Effect of the Anchoring Strength on the Phase Behaviour of Discotic Liquid Crystals under face-on Confinement. *J. Phys.: Condens. Matter* **2019**, *31*, 105101.
(21) Teixeira, P. I. C.; Anquetil-Deck, C.; Cleaver, D. J. Ordering of Oblate Hard Particles Between Symmetric Penetrable Walls. *Liq. Cryst.* **2020**, in press.
(22) Sluckin, T. J. The Liquid Crystal Phases: Physics and Technology. *Contemp. Phys.* **2010**, *41*, 37−56.
(23) Bryan-Brown, G. P.; Wood, E. L.; Sage, I. C. Weak Surface Anchoring of Liquid Crystals. *Nature* **1999**, *399*, 338−340.
(24) Vandenbrouck, F.; Valignat, M. P.; Cazabat, A. M. Thin Nematic Films: Metastability and Spinodal Dewetting. *Phys. Rev. Lett.* **1999**, *82*, 2693−2696.
(25) Teixeira, P. I. C.; Barmes, F.; Cleaver, D. J. Symmetric Alignment of the Nematic Matrix Between Close Penetrable Colloidal Particles. *J. Phys.: Condens. Matter* **2004**, *16*, S1969.
(26) Teixeira, P. I. C.; Barmes, F.; Anquetil-Deck, C.; Cleaver, D. J. Simulation and Theory of Hybrid Aligned Liquid Crystal Films. *Phys. Rev. E* **2009**, *79*, No. 011709.
(27) Teixeira, P. I. C. Nematic Liquid Crystal Order Reconstruction in Ultraconfinement, From Density-Functional Theory. *Liq. Cryst.* **2016**, *43*, 1526.
(28) Rigby, M. Hard Gaussian Overlap Fluids. *Mol. Phys.* **2006**, *68*, 687−697.
(29) Perram, J. W.; Wertheim, M. S. Statistical Mechanics of Hard Ellipsoids. I. Overlap Algorithm and the Contact Function. *J. Comput. Phys.* **1985**, *58*, 409−416.
(30) Allen, M. P.; Evans, G. T.; Frenkel, D.; Mulder, B. M. Hard Convex Body Fluids. *Adv. Chem. Phys.* **1993**, *86*, 1−166.
(31) Perram, J. W.; Rasmussen, J.; Praestgaard, E.; Lebowitz, J. L. Ellipsoid Contact Potential: Theory and Relation to Overlap Potentials. *Phys. Rev. E* **1996**, *54*, 6565−6572.
(32) Bhethanabotla, V. R.; Steele, W. A Comparison of Hard-Body Models for Axially-Symmetric Molecules. *Mol. Phys.* **2006**, *60*, 249−251.
(33) Huang, S.-L.; Bhethanabotla, V. R. Virial Coefficients for the Hard Gaussian Overlap Model. *Int. J. Mod. Phys. C* **1999**, *10*, 361−374.
(34) Velasco, E.; Mederos, L. A Theory for the Liquid-Crystalline Phase Behavior of the Gay-Berne Model. *J. Chem. Phys.* **1998**, *109*, 2361−2370.
(35) Cleaver, D. J.; Teixeira, P. I. C. Discontinuous Structural Transition in a Thin Hybrid Liquid Crystal Film. *Chem. Phys. Lett.* **2001**, *338*, 1−6.
(36) Telo da Gama, M. M. The Interfacial Properties of a Model of a Nematic Liquid-Crystal. *Mol. Phys.* **2006**, *52*, 611−630.
(37) Kaiser, P.; Wiese, W.; Hess, S. Stability and Instability of an Uniaxial Alignment against Biaxial Distortions in the Isotropic and Nematic Phases of Liquid Crystals. *J. Non-Equilib. Thermodyn.* **1992**, *17*, 153−169.
(38) Allen, M. P.; Tildesey, D. J. *Computer Simulation of Liquids*; Oxford University Press: Princeton (NJ), 2017.
(39) Geigenfeind, T.; Rosenzweig, S.; Schmidt, M.; De Las Heras, D. Confinement of Two-Dimensional Rods in Slit Pores and Square Cavities. *J. Chem. Phys.* **2015**, *142*, 174701.

https://dx.doi.org/10.1021/acs.jpcb.0c05027
J. Phys. Chem. B 2020, 124, 7709−7716